ARTICLE

Abnormal co-doping effect on the red persistent luminescence SrS:Eu^{2+},RE^{3+} materials

AbnReceived 00th January 20xx,
Accepted 00th January 20xx

DOI: 10.1039/x0xx00000x

Danilo Ormeni Almeida dos Santos,[a] Luidgi Giordano,[a] Miguel Aguirre Stock Grein Barbará,[a] Marcelo Cecconi Portes,[a] Cássio Cardoso Santos Pedroso,[b,c] Verônica Carvalho Teixeira,[d] Mika Lastusaari,[e] and Lucas Carvalho Veloso Rodrigues [a,*]

Persistent luminescence materials are a reality in several applications. However, efficient red-emitting materials are still lacking. SrS:Eu^{2+} phosphor keeps as a potential candidate since its strong nephelauxetic effect shifts $Eu^{2+}4f^65d^1 \rightarrow 4f^7$ to red and its weak bond between strontium and sulphide, due to the soft base-hard acid character, generate a high number of intrisic defects. The SrS:Eu^{2+},RE^{3+} materials were efficiently prepared by two rounds of 22 min microwave-assisted solid-state synthesis. The highly crystalline purity and the material organization at the micro-scale were observed with X-ray powder diffraction and Scanning Electron Microscopy, respectively. X-ray absorption spectroscopy pointed out a low ammount of Eu^{2+} compared to Eu^{3+} due to the efficient Eu^{2+} photo-oxidation by X-ray irradiation in the high storage capability SrS host matrix. Electron Paramagnetic Ressonance spectra confirmed that at least 50 % of Eu^{2+} ions in the material are photo-oxidized during excitation, reinforcing previously estabilished mechanisms. The RE^{2+} energy level positioned very close or into the conduction band led to an abnormal co-doping effect, with similar effect independent on the co-dopant. The high concentration of intrinsic defects in SrS indicates that soft-hard pair hosts is an excellent approach to develop efficient persistent luminescence materials.

1. Introduction

Alkaline earth sulphides can be considered the starting point of persistent luminescence, as the first reported persistent material, back in 1602 by Vincenzo Cascariolo was BaS:Cu^+ [1]. Studies involving the luminescence in these sulphides were developed by Lenard at the 20th century [2–4], and as such, doped CaS, SrS and BaS are also known as Lenard's phosphors. They are known for their low resistance to humidity and water [5], making them difficult to apply in different fields. To overcome this problem, studies of materials coating are leading to real-world applications e.g., improvement of algae photosynthetic activity [6,7].

There is a gap in the development of red-emitting persistent luminescence (red-PeL) materials which are more scarce and with less luminance when compared to the known blue- and green-emitting ones[8]**.** Known red-PeL materials are usually related to Sm^{3+}, Eu^{3+}, Mn^{2+}, Cr^{3+} or Pr^{3+} activators [9], while the most efficient materials for blue and green emission are commonly Eu^{2+}-doped materials[10]**.** The presence of Eu^{2+} as emitting-ion can be related to the higher efficiency for these colours, as Eu^{2+} emission has an allowed transition by Laporte's rule ($4f^65d^1 \rightarrow 4f^7$ transition), differently from all the activators mentioned above (f-f and d-d transitions). Therefore, the development of red-emitting Eu^{2+} materials can be a starting point to improve red-PeL solids.

In Eu^{2+} $4f^65d^1 \rightarrow 4f^7$ transition, the 5d energy-levels can be shifted in an easier manner in comparison to the atomic-like 4f level, as 5d orbital has strong interactions with the chemical environment. There are mainly two ways to get red emission from Eu^{2+}. The first manner is with high ligand field hosts, that increase the split of 5d levels and decrease the energy difference between the lowest 5d level and the 4f ground state. This is the case of $M_2Si_5N_8$:Eu^{2+} materials that exhibit reddish-PeL due to the high ligand field of nitride anion[11]. The second way is by high covalent materials, leading to a strong nephelauxetic effect decreasing 5d level energy, red-shifting the emission [9,10,12]. The advantage of europium doped alkaline earth sulphides is the strong nephelauxetic effect combined with the low ligand field leading to red emission and small 5d splitting, allowing efficient excitation with low energy light.

Persistent luminescence materials store energy in defects and the storage capacity is directly related to the concentration of thermal bleached defects [13]. There are two main groups of point defects that can be formed in a host: i) the intrinsic (Schottky or Frenkel), thermodynamically formed during heating of the material; and ii) extrinsic, formed by the insertion of alio- or even isovalent (co-)doping.

[a] *Department of Fundamental Chemistry, Institute of Chemistry, University of São Paulo, 05508-000, São Paulo – SP, Brazil.*
[b] *Department of Biochemistry, Institute of Chemistry, University of São Paulo, 05508-000, São Paulo – SP, Brazil*
[c] *Current Address: Molecular Foundry, Lawrence Berkeley National Laboratory, Berkeley, CA, USA, 94720*
[d] *Brazilian Synchrotron Light Laboratory (LNLS), Brazilian Center for Research in Energy and Materials (CNPEM), BR 13083-970, Campinas-SP, Brazil.*
[e] *Department of Chemistry, University of Turku, FI20014, Turku, Finland*
*lucascvr@iq.usp.br

†Electronic Supplementary Information (ESI) available: [details of any supplementary information available should be included here]. See DOI: 10.1039/x0xx00000x

In Eu^{2+} doped materials, the presence of another rare-earth (RE) co-dopant is studied in literature since Matsuzawa reignited persistent luminescence in 1996 with the discovery of $SrAl_2O_4:Eu^{2+},Dy^{3+}$. The presence of the co-dopant increases the duration of persistent luminescence more than four orders of magnitude, like Dy^{3+} co-doping in $SrMgSi_2O_7:Eu^{2+},RE^{3+}$ [14]. The co-dopant effect was heavily discussed, with the development of models to explain persistent luminescence in both co-doped and non-co-doped materials. It is believed that the co-dopant can act in two ways, even simultaneously, in some cases. The aliovalent co-dopant increases the lattice defect concentration due to charge compensation or stabilizes some intrinsic defects. Also, they act as electron-hole trapping sites, depending on their position relative to the valence and conduction bands [10,15–18].

The PeL material synthesis must achieve high temperatures to increase the concentration of intrinsic defects since the defect formation is enthalpically disfavoured and entropy driven. So, the microwave-assisted solid-state synthesis (MASS) is a convenient methodology to achieve high temperatures in a fast way, followed by a fast cooling needed to keep high defect concentration. We used this synthetic approach already used to prepare other PeL materials[19–21]. Despite the MASS is used to prepare different PeL materials, we report the sulphate reduction to sulphides without a controllable atmosphere. We provide the reducing atmosphere in an open system by the incomplete combustion of activated carbon (also used as a susceptor), necessary for the reduction of sulphate to sulphide, and Eu^{3+} to Eu^{2+}.

In this work, a broad picture on the persistent luminescence behaviour of $SrS:Eu^{2+},RE^{3+}$ is studied. Based on low and high energy electronic spectroscopies as well as Electron Paramagnetic Resonance (EPR), to study the photo-oxidation of Eu^{2+} during excitation, we discuss the advantages of SrS as a good host for red persistent luminescence.

2. Experimental

2.1 Microwave-assisted solid-state synthesis (MASS)

The $SrS:Eu^{2+},RE^{3+}$ materials (1 mol-% of Eu^{2+} and 1–2 mol-% of RE^{3+}) were prepared from $SrSO_4$, $EuOHCO_3$, RE_2O_3 and S (in excess of 10 mol-%). The strontium sulphate salt was prepared via precipitation method starting from $SrCl_2$ (99.0 % Synth) in sulfuric acid (98.0 % Reagen). The precipitate was filtered, washed thoroughly with distilled water, and dried at 100˚C for 12 h. The $Eu(OH)CO_3$ was prepared via co-precipitation method starting from $EuCl_3.6H_2O$ and urea. The precipitate was washed three times with distilled water and separated by centrifugation. The pellet was resuspended in isopropanol and separated by centrifugation for posterior drying. Differently of Obut [22] that mixed the charcoal with $SrSO_4$, we chose to keep the precursors separated to avoid contamination. The reactants mixture was added to a small alumina crucible (5 cm^3), which was placed inside a larger alumina crucible (50 cm^3) filled previously with granular activated carbon (1-2 mm Synth). The crucible pair was partially closed with an alumina lid [19–21]. The system was properly allocated in a domestic microwave oven within a thermal aluminosilicate insulation block, in order to conceal the heat and prevent any damages to the microwave oven. As the final step, the precursors were heated for 12 and 10 minutes at power levels of 1000 and 900 W, respectively. The product obtained was homogenized and ground in an agate mortar, and the heating step was repeated following the same microwave oven program.

2.2 Characterization

Conventional X-ray Powder Diffraction measurements were made in a Bruker D2 PHASER Benchtop XRD using Cu Kα radiation (λ = 1.5406 Å) and 15 rpm rotation to avoid preferred orientation. The Scanning Electron Microscopy (SEM) was performed with FEI Inspect F50 available at the Brazilian Nanotechnology National Laboratory (LNNano, Brazilian Center for Research in Energy and Materials (CNPEM), Campinas-SP, Brazil) with 5 keV voltage and Spotsize 2.

EPR measurements were carried out in a continuous wave Bruker EMX equipment at X-Band (9,5Ghz) with 20mW power and 7G of modulation amplitude with a standard cavity. The solid samples were accommodated at a 3mm diameter quartz tube at room temperature (RT). A 405nm laser perpendicular to the cavity was used to perform analysis under irradiation. EPR simulations was generated in EasySpin [23] software attached to Matlab.

The X-ray Absorption Spectroscopy at Sulphur K-edge and Eu L_3-edge experiments were measured, respectively, at the Soft X-Ray Spectroscopy (SXS) and X-Ray Absorption and Fluorescence Spectroscopy (XAFS2) beamlines of the Brazilian Synchrotron Light Laboratory (LNLS - CNPEM), Campinas-SP, Brazil. A Si (111) monochromator was used for the measurement at Sulphur K-edge and the absorption correction was done using an Al foil. The sample was added to a carbon conductive tape attached to a steel sample holder. The system was kept at 5 10^{-8} mbar, connected to a copper wire and the X-ray Absorption Near Edge Structure (XANES) data was obtained in total electron yield (TEY) mode using a Keithley 6514. For the spectrum at the Eu L_3-edge, it was used a Si (111) double monochromator. The sample was prepared as a pellet and the XANES spectrum was measured in fluorescence mode using a solid state 15-channel Germanium detector.

Luminance measurements were carried out after 10 min irradiation of 6 W 300 nm Hg lamp in a Hagner ERP – 05 luminance photometer until the 0.32 mcd/m^2 counting, the luminance threshold for applications and around 100 times the sensitivity of human eye adapted to dark[24]. Thermoluminescence (TL) was measured in a MikroLab Thermoluminescent Materials Laboratory Reader RA'04. Prior to the TL experiments, the samples were irradiated by a 6 W 300 nm Hg lamp for 5 min, and the glow curve was registered 30 s after ceasing the irradiation. Excitation and emission spectroscopy measurements in UV-visible range were obtained in a Horiba Fluorolog 3. Vacuum ultra-violet (VUV) spectroscopy measurements were performed at the Toroidal Grating Monochromator (TGM) beamline from the Brazilian Synchrotron Light Laboratory (LNLS), with quartz (4.5 – 8.5 eV)

filter to avoid higher harmonics excitation[25]. The total emission was collected using an optical fibre coupled to a Hamamatsu R928 photomultiplier. A low-pass filter (305 nm) was used in front of the photomultiplier and the signal was corrected by the sodium salicylate spectrum [26]. The emission spectra were registered with the same configuration using an Ocean Optics QE65000 spectrometer instead of the set low-pass filter and photomultiplier.

3. Results and Discussion

3.1 Structure, morphology and valence characterization

The activated carbon used as microwave susceptor in the MASS generates CO locally, which has a highly reducing character. It is crucial for the precursors' reduction to sulphide and Eu^{2+}.

The XRD measurement of $SrS:Eu^{2+},Sm^{3+}$ after one heating cycle (Fig. 1) shows a massive presence of $SrSO_4$. When the same material is ground and homogenized after the first cycle and heated again, the XRD exhibit SrS cubic diffraction peaks without crystalline impurities. Based on this result, all materials with different co-dopants were synthesized with two heating rounds and showed the same XRD pattern (Fig. S1). The presence of small intensity peaks around 31°, even after the second heat (Fig S1), are probably from $SrSO_4$ impurities present due to surface oxidation, but the small intensity makes a clear assignment difficult. The presence of europium did not lead any observable rare earth enriched phases. This is because europium is well soluble to the Sr sites due to the similarity between their valence and ionic radii (Sr^{2+}: 1.18 Å and Eu^{2+}: 1.17 Å, both with coordination number 6) [27]. For the co-dopants, even if there is a charge mismatch (that create defects via charge compensation); and a considerable size difference (Ce^{3+}-Yb^{3+}: 1.01-087 Å), there is no evidence of phase segregation. This suggests that the co-dopant concentration is low enough to allow solid solubility, or that the content of the possibly segregated phases is below the detection limit of XRD.

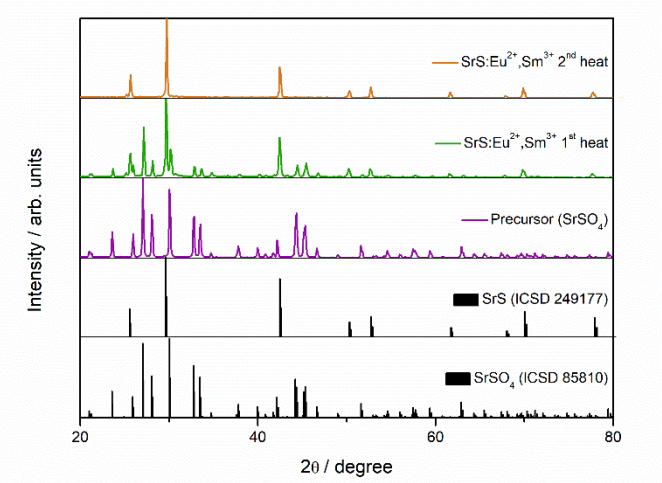

Fig. 1. X-ray diffraction pattern of microwave assisted synthesized $SrS:Eu^{2+},Sm^{3+}$ with one and two heating cycles by MASS.

The SEM images show that the synthesis formed aggregates with more than 10 µm (Fig. 2a). These aggregates are formed by particles with different sizes ranging from hundreds of nanometres to micrometres (Fig 2b). This broad particle distribution is an indication that Ostwald Ripening took place [28].

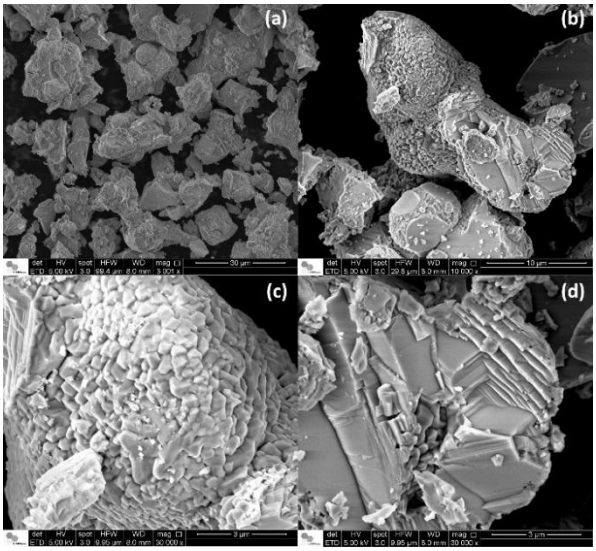

Fig. 2. Scanning Electron Microscopy of the microwave assisted synthesized $SrS:Eu^{2+},Sm^{3+}$ with a) 3000, b) 10000 and c, d) 30000 magnification.

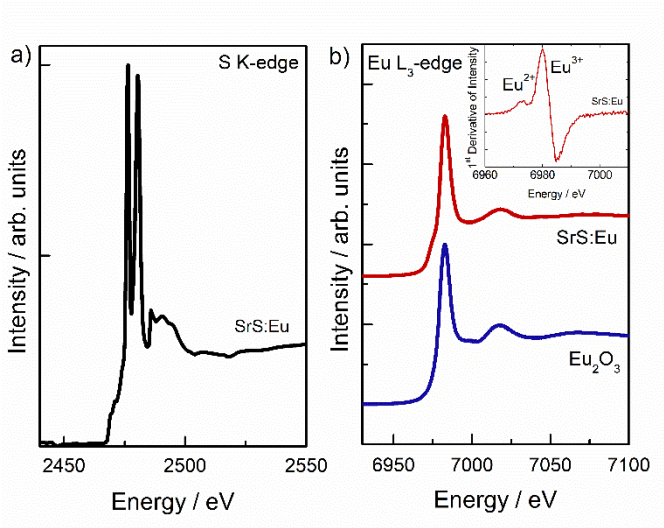

Fig. 3. X-ray absorption spectra of SrS:Eu at the a) S K-edge and b) Eu L_3-edge. In the inset the 1st derivative of Eu L_3 XANES.

This is expected due to high temperatures achieved in the microwave, melting the sulphur precursor, and already observed in RE_2O_2S synthesis by MASS[19]. Both the small and large particles present pointed shapes, differently from other synthesis methods like sol-gel [29] (Figs 2c and 2d).

The X-ray absorption spectrum in XANES region of $SrS:Eu^{2+}$ at the sulphur K-edge (Fig 3a) exhibits two strong peaks at 2476 and 2480 eV and a band close to 2485 eV. The attribution of sulphur XANES is not a simple task, mainly due to the high covalent character of sulphide and the intense peak shifts induced by the material composition. Farrel et al. [30] show that the sulphide characteristic pre-edge absorption can vary from 2470 eV in high covalent material, e.g. FeS, to 2474 eV in the more ionic CaS. Besides, they observe the edge absorption up to 2480 eV in different sulphides. Considering these empirical

results, the peak at 2476 eV is related to the pre-edge transition from S $1s^2$ to a hybridized state formed by S 3p σ* antibonding and Sr low-lying 4d levels. The 2480 eV is the edge transition from S $1s^2$ to S 3p σ* antibonding state. The band observed close to 2485 eV is attributed to sulphate edge absorption. We suggest a surface oxidation, similarly observed in RE_2O_2S materials [19].

The XANES spectrum in the Eu L_3-edge indicates that the majority of Eu is in trivalent state with the peak at 6983 eV, while the presence of divalent europium is only clearly observed in the derivative curve (Fig 3b, inset). This is not compatible with the bright orange colour of the material (Fig S2) that arises from Eu^{2+} absorption in the blue-green region and with the very efficient persistent luminescence of the phosphor as it will be seen in the following section. Besides, Eu^{2+} should be very stable in the SrS host since Eu^{2+} has the same charge/radius as Sr^{2+} and is a softer acid than Eu^{3+}, interacting better with the sulphide soft base [31]. The main problem with XANES of Eu in several persistent luminescence materials is the photo-oxidation that might take place if the material is efficiently excited with X-rays, which is exactly the case with SrS:Eu^{2+}. Besides, it was already shown that X-ray irradiation can also cause permanent oxidation due to radiation damage [32].

In order to study Eu valence and the effect of light on it, the EPR spectra were measured in the absence and presence of 405 nm laser (Fig. 4). EPR is a sensitive technique to measure the concentration of occupied vacancies or the concentration of some problematic ions, e.g., Ti^{3+} [33]. The advantage of EPR is that is a method that, itself, cannot change the oxidation state of the metal, differently from X-ray absorption.

The EPR spectrum of SrS:Eu^{2+} (Fig. 4a) shows the expected EPR signal for divalent europium species, considering the isotopic distribution of Europium, 151 (48%) and 153 (52%), both species with nuclear spin of 5/2. Europium should present 12 peaks in EPR (two sextets due to the two active isotopes), however the EPR spectrum exhibits 13 peaks and shoulders, which is not compatible with only one Eu^{2+} site [34]. Using the EPR simulation, it can be established the presence of two different Eu^{2+} sites, both species with the same g value of 1.9995, presenting different values only for the hyperfine coupling constant. The simulation determined that the hyperfine coupling constant values are 14.3G and 46.5G, both octahedral. The two species can be attributed either to the presence of little quantities of sulphate, as shown on XANES technique or due to the presence of defects close to Eu^{2+} sites.

When the sample is irradiated by a 405nm laser (Fig. 4b; under the same conditions as without light), it was observed a decrease of 49% on the Eu^{2+} signal using the double integration (with WinEPR 2.11 software). This result proves that Eu^{2+} is being photo-oxidized to Eu^{3+}, which is EPR silent, during the charging of persistent luminescence. The decrease of almost half of Eu^{2+} concentration may explain the almost absence of Eu^{2+} in XANES. In EPR, the irradiation was only on the surface of the bulk but X-rays can penetrate deeper than blue light, increasing the amount of Eu^{2+} photo-oxidized.

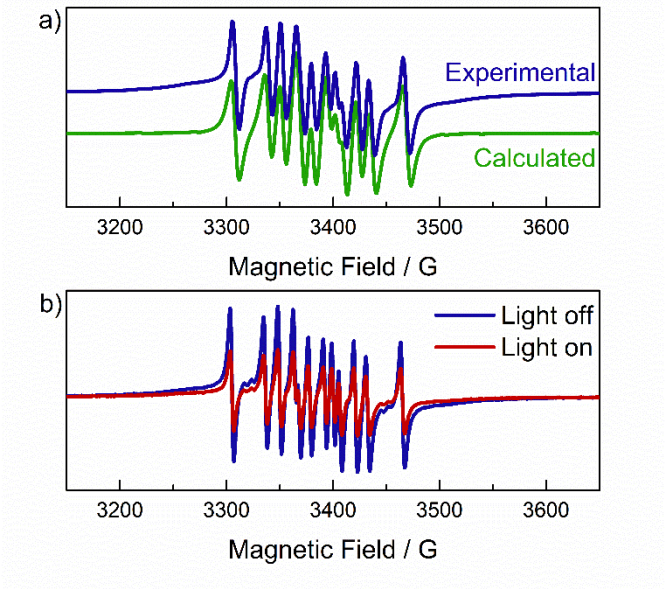

Fig. 4. a) EPR spectra (experimental and calculated) of SrS:Eu^{2+}. b) Effect of 405 nm laser on SrS:Eu^{2+} EPR spectra.

3.2 Persistent Luminescence

The emission spectrum of SrS:Eu^{2+} (Fig. 5) prove that in the presence of sulphide anion, the typically blue-green emission of Eu^{2+} is redshifted. The $4f^65d^1 \rightarrow 4f^7$ emission of Eu^{2+} in this material is centred around 620 nm due to the strong nephelauxetic effect. It is also observed the low stokes shift, leading to an excitation band in the blue-green region, important for several applications like white LEDs. The low

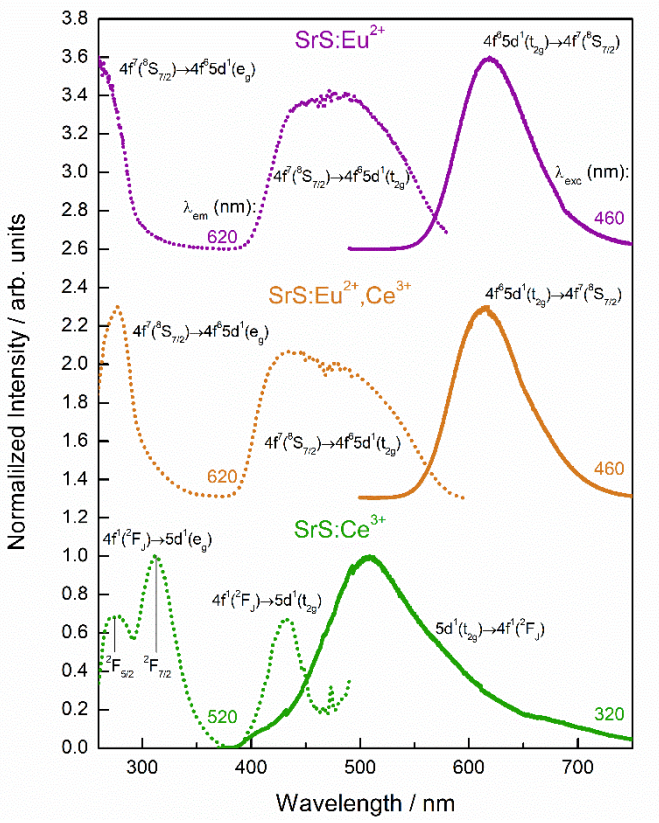

Fig. 5. Excitation and emission spectra of SrS:Eu^{2+}, SrS:Eu^{2+},Ce^{3+} and SrS:Ce^{3+}.

crystal field of the octahedral site, around 13,000 cm^{-1}, is in agreement with the value found for Yb^{2+}-doped SrS by Parmentier et al. [35] and leads to a small splitting between e_g and t_{2g} states. It must be noted that the t_{2g} state is overlapped with the band gap absorption. The strong nephelauxetic effect also redshifts Ce^{3+} emission to 500 nm, likewise in nitrides [36].

The spectra of SrS:Eu^{2+},Ce^{3+} material are dominated by Eu^{2+} bands and low contribution of Ce^{3+} transitions. Even if Ce^{3+} can also emit in red region, there is no clear difference in the Eu^{2+} 620 nm band with Ce-co-doping [37,38]. Since the excitation bands of Ce^{3+} and Eu^{2+} are overlapped, the energy transfer from cerium to europium is highly probable. For all the other co-dopants, the emission spectra under excitation above the band gap exhibits only the Eu^{2+} band at 620 nm (Fig S3) like observed for the majority of Eu^{2+},RE^{3+} co-doped materials [14].

Since the band gap absorption of the SrS semiconductor is just at the limit of conventional Xe-lamp excitation, the VUV spectra were registered to evaluate the host matrix contribution in the Eu^{2+}-doped materials spectra (Fig. 6). The spectra are very similar among each other and no apparent difference (larger than the ±0.05 eV resolution) is observed with different co-dopants. The value of the first derivative maximum, 4.55 eV, agrees with the band gap reported in the literature (4.65 eV) [39].

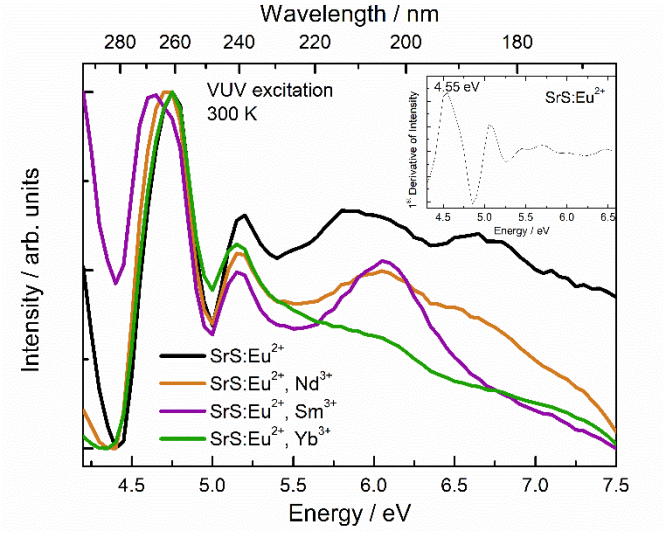

Fig. 6. VUV excitation spectra of SrS:Eu^{2+},RE^{3+}. In the inset, the 1st derivative of the SrS:Eu2+ curve.

The persistent luminescence decay time for the SrS-based materials was recorded until the luminance was at 0.32 mcd/m^2 the limit of the human eye adapted to the dark (Fig. 7). Even if red emission is not in the optimal region of the eye sensibility in the dark and the storage capacity of the phosphor will be probably be underestimated [13], this data allows to understand the effect of the co-dopant in SrS:Eu^{2+},RE^{3+} PeL mechanism. The luminance measurements indicate that persistent luminescence of SrS:Eu^{2+} increases from 13 min to 60 min when co-doped with 1mol-% of RE^{3+} (except Ce^{3+}) and to 75 min with 2mol-% of co-dopant. With Ce^{3+} as co-dopant, the increase on persistent luminescence is smaller, up to 40 min (independent on its concentration). Since no Ce^{3+}-PeL is observed for SrS:Eu^{2+},Ce^{3+} material, no path from Eu^{2+} to Ce^{3+} should occur.

The SrS:Ce^{3+} PeL is very short, it can be justified by the faster lifetime of Ce^{3+} emitting state (ns) than Eu^{2+} ones (µs). So, the probability of Ce^{3+} emission under excitation is higher than the chance of electron trapping formation. Thus, since there is no evidence on the PeL energy transfer from Ce^{3+} to Eu^{2+}, the discrepancy on Eu^{2+},Ce^{3+}-doped PeL might be due to a

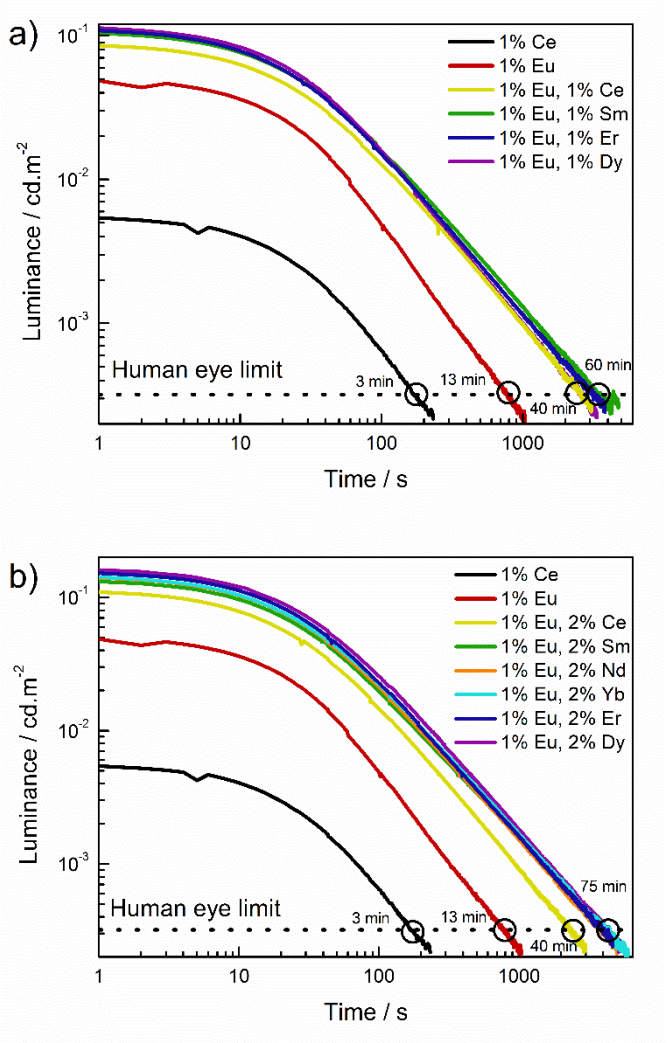

Fig. 7. Persistent luminescence decay time of SrS:Eu^{2+},RE^{3+} and SrS:Ce^{3+} materials with co-doping concentrations of a) 1% and b) 2%.

competition between charging and non-radiative decay, reducing the concentration of trapped charge carriers.

The increase of only less than 6 times in the persistent luminescence decay when the material is co-doped with RE^{3+} ions and the similarity on the persistent luminescence time, independent on the co-dopant, is completely discrepant of other Eu^{2+} doped materials as $CaAl_2O_4$:Eu^{2+},RE^{3+}, $BaAl_2O_4$:Eu^{2+},RE^{3+} or $SrMgSi_2O_7$:Eu^{2+},RE^{3+} (2, 3 and 4 orders of magnitude, respectively) and also non Eu^{2+} co-doped materials like the YPO_4:Ce^{3+},RE^{3+} (4 orders of magnitude)[14,18,40,41]. Two reasons behind this anomalous behaviour are the position of the energy states of the co-dopants and the defect concentration in SrS material. Dorenbos[16] and Bos et al [41] proposed that the RE^{3+} co-dopants act as electron traps, forming RE^{2+} and thermal energy release the trapped electron generating persistent luminescence. The energy of the RE^{2+}

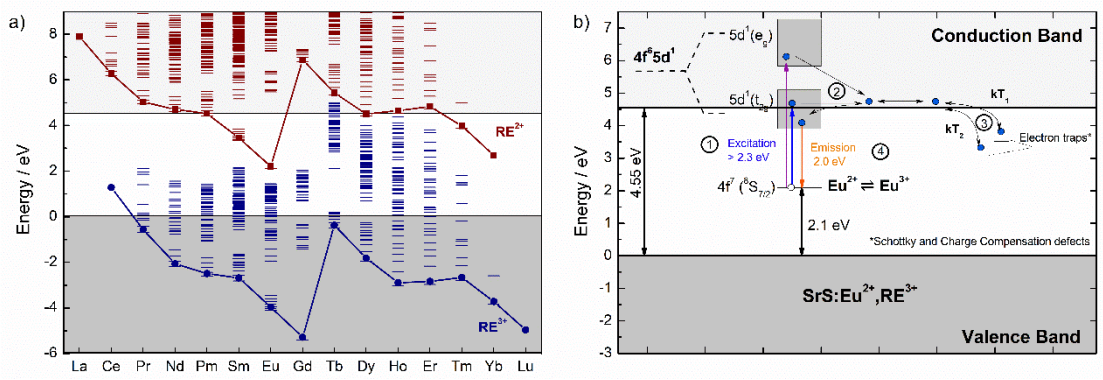

Fig. 8. a) Host-Referred 4f-electron Binding Energy curves and excited state energies of RE^{2+} and RE^{3+} ions in SrS. b) Persistent luminescence mechanism for Eu^{2+} in SrS.

ground levels relative to the bottom of the conduction band is, thus, related to the thermal energy needed. In SrS, the position of the RE^{2+} energy levels can be determined (Fig. 8a) using the Host Referred 4f-electrons Binding Energy (HRBE) curves (derived from the Vacuum Referred 4f-electrons Binding Energy – VRBE curves) [42]. These curves can be determined from the band gap energy, as well as the Eu^{3+} charge transfer transition (from the literature) using the methodology proposed by Dorenbos [39,42]. It can be observed that all the ground state of all RE^{2+} ions, except Sm, Eu, and Yb is inside (or very closed to) the conduction band, not allowing these ions to act as electron traps. So, it would be expected that only Sm or Yb to be able increase significantly the persistent luminescence. However, this is not the case, mainly because these divalent ions are very stable in this host, and the reduction atmosphere might reduce the amount of the trivalent co-dopants. As a result, the only effect by co-doping should be the creation of charge compensation defects, and since all the rare earth co-dopants present similar ionic radii, the defects should be similar. The RE^{3+} co-dopants might be present as clusters in distorted sites, as observed by Mahlik et al. for Ce^{3+}-doped SrS materials [37]. The thermoluminescence glow curves (Fig. S4) show that the co-dopants might not create different room temperature accessible defects from what is observed in only Eu^{2+}-doped material. Of course, it must be noted that they may create high temperature defects that do not lead to room temperature PeL. The broadening of the 80 °C centred TL band could be due to the presence of different defects with similar energy but in order to get more details several TL studies are needed, which is out of the scope of this work.

Even if the co-doping generates more defects, it is observed that the increase in persistent luminescence is not even 1 order of magnitude. The reason is the already high concentration of intrinsic defects in SrS even without any co-dopant. This high concentration is related to the weak bond between strontium and sulphide since strontium is a hard acid and sulphide a soft base, which decreases the defect formation energy. Pandey et al.[43] calculated theoretically the formation energy for the intrinsic defects, finding 7.0 eV for the Schottky pair defect as well as 14.2 eV for S^{2-} and 9.6 eV for Sr^{2+} Frenkel defects. This indicates that the formation of a pair of Sr^{2+} and S^{2-} vacancies is more favourable than the formation of Frenkel defects, mainly because the ions are much larger than the interstitial sites. By using statistical thermodynamics, it is possible to estimate the defect concentration at different temperatures. The defect molar fraction (X_D) can be determined by equation 1 where ϵ_D is the formation energy of the defect, k is the Boltzmann constant and T the temperature [44].

$$X_D = e^{\frac{-\epsilon_D}{2kT}} \qquad \text{(Eq. 1)}$$

At room temperature the molar fraction (in defects/sites – where the sites are relative to strontium and sulphide) of Schottky defects would be very low ($2x10^{-60}$ defects/sites leading to a concentration of $1x10^{-36}$ defects/mol). However, if the synthesis temperature is considered (about 1500 K, according to estimative made by Carvalho et al)[19] a considerably high concentration of $1x10^{12}$ defects/mol is found. Since the cooling is fast and the ionic mobility is very low at room temperature, this defect concentration should not decrease considerably. If it is considered ideally that each defect can store on electron (and consequently, 1 photon) this value is still around four orders of magnitude when compared to $CaSEu^{2+}$ nanoparticle with $5x10^{16}$ photon/mol [13]. Thus we consider that the microwave synthesis is ideal to form high defect concentration, but extrinsic defects must also be induced in order to have efficient persistent luminescence materials.

Based on the data shown in this work, a schematic mechanism can be obtained (Fig 8b). After the irradiation at the $4f^7 \rightarrow 4f^65d^1$ transition of Eu^{2+} in the blue-green or UV region (1), Eu^{2+} is photo-oxidized with the electron escaping to the conduction band (2). The electron is then trapped in the intrinsic defects or those formed via charge compensation by the co-dopant insertion (which increases the energy storage capacity) and this electron can return to the conduction band with the aid of thermal energy (3). The recombination of the electron with europium restore the Eu^{2+} emitting centre leading to radiative emission, generating red persistent luminescence (video in supplementary material).

Conclusions

The efficient $SrS:Eu^{2+},RE^{3+}$ red persistent luminescence materials were conveniently synthesized with the microwave-assisted solid-state method. XANES turned out to be a poor

technique to analyse Eu^{2+} presence in materials that present efficient persistent luminescence under X-ray irradiation. EPR spectroscopy indicated that at least half of Eu^{2+} photo-oxidize under blue laser irradiation. Besides, this technique allows excitation with different radiation, which is convenient for oxidation state studies in PeL materials. The high concentration of intrinsic defects in SrS host material is justified by the weak interaction of the hard acid and soft base. The effect of RE^{3+} co-dopant just increases defects via charge compensation. No new traps for PeL at room temperature are generated via RE^{3+} co-doping. Similar PeL increment is observed independently of the RE^{3+} co-dopant, except for Ce^{3+}, which is explained by competition between PeL charging and luminescence under excitation.

Conflicts of interest

There are no conflicts to declare.

Acknowledgements

The authors thank the financial support of FAPESP - São Paulo Research Foundation, Brazil (CCSP scholarship #2017/09774-0 and LCVR project #2018/05280-5), CNPq – National Council for Scientific and Technological Development, Brazil (DOAS, LG and MASGB scholarships #133123/2016-2, #141252/2017-0 and #132148/2016-1, LCVR Projects #490242/2012-0, #427312/2016-7) and CAPES - Coordenação de Aperfeicoamento de Pessoal de Nível Superior, Brazil (CCSP). The authors also acknowledge the CNPEM for the beamtime at SXS (#20170354), XAFS2 (#20170868) and TGM (#20180001) beamlines of LNLS and the Microscope time at LNNano (#23479). The support of the CNPEM staff is also acknowledge, in special Dr. Flavio Vicentin, Dr. Douglas Galante, Dr. Santiago Alejandro Figueroa, Dr. Anna P.S. Sotero, Eng. Felipe Del Nero, Eng. Leonardo Mitsuo Kofukuda Mr. Junior Cintra Mauricio, for the kind attention and valuable discussion around the collected data. The authors are grateful to Prof. Ana Maria da Costa Ferreira for the access to EPR instrument, supported by CEPID-Redoxoma Network (FAPESP #2013/07937-8). Prof. Hermi F. Brito is kindly acknowledged for the Fluorometer and for support and advices in the beginning of LCVR career.

References

1 M. Lastusaari, T. Laamanen, M. Malkamäki, K. O. Eskola, A. Kotlov, S. Carlson, E. Welter, H. F. Brito, M. Bettinelli, H. Jungner and J. Hölsä, *Eur. J. Mineral.*, 2012, **24**, 885–890.

2 V. Klatt and P. Lenard, *Uber die Phosphoreszenzen des Kupfers Wismuths und Mangans in den Erdalkalisulfiden*, 1889.

3 P. Lenard and V. Klatt, *Ann. Phys.*, 1904, **13**, 425–484.

4 P. Lenard and V. Klatt, *Ann. Phys.*, 1904, **12**, 225–282.

5 H. F. Brito, J. Hölsä, T. Laamanen, M. Lastusaari, M. Malkamäki and L. C. V. Rodrigues, *Opt. Mater. Express*, 2012, **2**, 371.

6 C. Guo, B. Chu, M. Wu and Q. Su, *J. Lumin.*, 2003, **105**, 121–126.

7 L. Wondraczek, M. Batentschuk, M. A. Schmidt, R. Borchardt, S. Scheiner, B. Seemann, P. Schweizer and C. J. Brabec, *Nat. Commun.*, 2013, **4**, 2047.

8 Y. Zhuang, Y. Katayama, J. Ueda and S. Tanabe, *Opt. Mater. (Amst).*, 2014, **36**, 1907–1912.

9 K. Van Den Eeckhout, D. Poelman and P. F. Smet, *Materials (Basel).*, 2013, **6**, 2789–2818.

10 K. Van den Eeckhout, P. F. Smet and D. Poelman, *Materials (Basel).*, 2010, **3**, 2536–2566.

11 K. Van den Eeckhout, P. F. Smet and D. Poelman, *Materials (Basel).*, 2011, **4**, 980–990.

12 P. Dorenbos, *J. Lumin.*, 2003, **104**, 239–260.

13 D. Van der Heggen, J. J. Joos, D. C. Rodríguez Burbano, J. A. Capobianco and P. F. Smet, *Materials (Basel).*, 2017, **10**, 1–13.

14 M. Lastusaari, H. Jungner, A. Kotlov, T. Laamanen, L. C. V. Rodrigues, H. F. Brito and J. Hölsä, *Zeitschrift für Naturforsch. B*, 2014, **69**, 171–182.

15 J. Xu and S. Tanabe, *J. Lumin.*, 2019, **205**, 581–620.

16 P Dorenbos, *phys. stat. sol.*, 2005, **242**, 7–9.

17 T. Aitasalo, J. Ho, M. Lastusaari and J. Niittykoski, *J. Phys. Chem. B*, 2006, **110**, 4589–4598.

18 L. C. V. Rodrigues, J. Hölsä, J. M. Carvalho, C. C. S. Pedroso, M. Lastusaari, M. C. F. C. Felinto, S. Watanabe and H. F. Brito, *Phys. B Condens. Matter*, 2014, **439**, 67–71.

19 J. Miranda De Carvalho, C. C. S. Pedroso, I. P. Machado, J. Hölsä, L. C. V. Rodrigues, P. Głuchowski, M. Lastusaari and H. F. Brito, *J. Mater. Chem. C*, 2018, **6**, 8897–8905.

20 I. P. Machado, C. C. S. Pedroso, J. M. de Carvalho, V. de C. Teixeira, L. C. V. Rodrigues and H. F. Brito, *Scr. Mater.*, 2019, **164**, 57–61.

21 C. C. S. Pedroso, J. M. Carvalho, L. C. V. Rodrigues, J. Hölsä and H. F. Brito, *ACS Appl. Mater. Interfaces*, 2016, **8**, 19593–19604.

22 A. Obut, *Miner. Eng.*, 2007, **20**, 1320–1322.

23 S. Stoll and A. Schweiger, *J. Magn. Reson.*, 2006, **178**, 42–55.

24 D. Poelman, N. Avci and P. F. Smet, *Opt. Express*, 2009, **17**, 358.

25 R. L. Cavasso Filho, A. F. Lago, M. G. P. Homem, S. Pilling and A. Naves de Brito, *J. Electron Spectros. Relat. Phenomena*, 2007, **156–158**, 168–171.

26 D. Dutczak, T. Jüstel, C. Ronda and A. Meijerink, *Phys. Chem. Chem. Phys.*, 2015, **17**, 15236–15249.

27 R. D. Shannon, *Acta Crystallogr. Sect. A*, 1976, **32**, 751–767.

28 M. Kahlweit, *Adv. Colloid Interface Sci.*, 1975, **5**, 1–35.

29 S. S. Pitale, S. K. Sharma, R. N. Dubey, M. S. Qureshi and M. M. Malik, *Opt. Mater. (Amst).*, 2009, **31**, 923–930.

30 S. P. Farrell, M. E. Fleet, I. E. Stekhin, A. Kravtsova, A. V. Soldatov and X. Liu, *Am. Mineral.*, 2002, **87**, 1321–1332.

31 R. G. Pearson, *J. Chem. Educ.*, 1987, **64**, 561.

32 L. Amidani, K. Korthout, J. J. Joos, M. Van Der Linden, H. F. Sijbom, A. Meijerink, D. Poelman, P. F. Smet and P. Glatzel, *Chem. Mater.*, 2017, **29**, 10122–10129.

33 I. Norrbo, J. M. Carvalho, P. Laukkanen, J. Mäkelä, F.

Mamedov, M. Peurla, H. Helminen, S. Pihlasalo, H. Härmä, J. Sinkkonen and M. Lastusaari, *Adv. Funct. Mater.*, 2017, **27**, 1606547.

34 V. Jarý, L. Havlák, J. Bárta, M. Buryi, M. Rejman, M. Pokorný, C. Dujardin, G. Ledoux and M. Nikl, *ECS J. Solid State Sci. Technol.*, 2020, **9**, 016007.

35 A. B. Parmentier, J. J. Joos, P. F. Smet and D. Poelman, *J. Lumin.*, 2014, **154**, 445–451.

36 J. W. H. van Krevel, H. T. Hintzen, R. Metselaar and A. Meijerink, *J. Alloys Compd.*, 1998, **268**, 272–277.

37 S. Mahlik, T. Lesniewski, M. Grinberg, D. Kulesza and E. Zych, *Phys. Chem. Chem. Phys.*, 2018, **20**, 10266–10274.

38 E. Zych, D. Kulesza, J. Zeler, J. Cybińska, K. Fiaczyk and A. Wiatrowska, *ECS J. Solid State Sci. Technol.*, 2016, **5**, R3078–R3088.

39 P. Dorenbos, *J. Phys. Condens. Matter*, 2003, **15**, 4797–4807.

40 T. Aitasalo, J. Hölsä, H. Jungner, M. Lastusaari and J. Niittykoski, *J. Phys. Chem. B*, 2006, **110**, 4589–4598.

41 A. J. J. Bos, P. Dorenbos, A. Bessière, A. Lecointre, M. Bedu, M. Bettinelli and F. Piccinelli, *Radiat. Meas.*, 2011, **46**, 1410–1416.

42 P. Dorenbos, *Phys. Rev. B*, 2012, **85**, 165107.

43 R. Pandey, A. B. Kunz and J. M. Vail, *J. Mater. Res.*, 1988, **3**, 1362–1366.

44 Donald R. Olander, *Fundamental aspects of nuclear reactor fuel elements*, 1977, vol. 68.

